Site- and bond-percolation thresholds in K_{n,n}-based lattices: Vulnerability of quantum annealers to random qubit and coupler failures on chimera topologies

O. Melchert, Helmut G. Katzgraber, and M. A. Novotny

Phys. Rev. E **93**, 042128 — Published 25 April 2016

DOI: 10.1103/PhysRevE.93.042128

Site and bond percolation thresholds in $K_{n,n}$-based lattices: Vulnerability of quantum annealers to random qubit and coupler failures on Chimera topologies

O. Melchert,[1] Helmut G. Katzgraber,[1,2,3] and M. A. Novotny[4,5]

[1]*Department of Physics and Astronomy, Texas A&M University, College Station, Texas 77843-4242, USA*
[2]*Santa Fe Institute, 1399 Hyde Park Road, Santa Fe, New Mexico 87501 USA*
[3]*Applied Mathematics Research Centre, Coventry University, Coventry, CV1 5FB, England*
[4]*Department of Physics and Astronomy, Mississippi State University, Mississippi State, MS 39762-5167, USA*
[5]*HPC^2 Center for Computational Sciences, Mississippi State University, Mississippi State, MS 39762-5167, USA*

We estimate the critical thresholds of bond and site percolation on nonplanar, effectively two-dimensional graphs with Chimera-like topology. The building blocks of these graphs are complete and symmetric bipartite subgraphs of size $2n$, referred to as $K_{n,n}$ graphs. For the numerical simulations we use an efficient union-find based algorithm and employ a finite-size scaling analysis to obtain the critical properties for both bond and site percolation. We report the respective percolation thresholds for different sizes of the bipartite subgraph and verify that the associated universality class is that of standard two-dimensional percolation. For the canonical Chimera graph used in the D-Wave Inc. quantum annealer ($n = 4$), we discuss device failure in terms of network vulnerability, i.e., we determine the critical fraction of qubits and couplers that can be absent due to random failures prior to losing large-scale connectivity throughout the device.

PACS numbers: 64.60.ah,64.60.F-,07.05.Tp,64.60.an

I. INTRODUCTION

In its most basic variant, the standard percolation model comprises a very minimalistic model of porous media [1–3]. However, despite its simplicity, percolation can be applied to problems across disciplines ranging from forest fires to current flow in resistor networks, liquid gelation, network connectivity, coffee brewing, simple configurational statistics [4], transport phenomena in ionic glasses [5], string-bearing models that also involve a large degree of optimization, describing, for example, vortices in high T_c superconductivity [6, 7], to name a few. Although conceptually simple, the configurational statistics of the percolation problem feature a nontrivial phase transition [8, 9]. To facilitate intuition, consider, for example, random-bond percolation on a two-dimensional square lattice where one studies a diluted system in which only a random fraction p of the edges subsist. The connected components [10] of the lattice can be seen as clusters that are then analyzed with respect to their geometric properties. Depending on the fraction p of subsisting edges, the geometric properties of the clusters change: Exceeding a lattice-structure dependent critical threshold p_c, the model transitions from a disconnected phase with typically small clusters to a phase where there is a single large cluster that interconnects a finite, nonzero fraction of the lattice sites, thus achieving large-scale connectivity. The appearance of this system-spanning cluster can be described by a second-order phase transition [11].

Because the location of the percolation critical point is sensitive to the topology of the underlying graph, there is general interest in understanding these threshold values for relevant model systems [12, 13]. In some cases it is possible to derive these thresholds exactly by analytical calculations. For example, in Refs. [14] and [15] a generating function approach was developed to determine the statistical properties of random graphs with arbitrary degree distribution (e.g., Erdős-Rényi random graph ensembles). Unfortunately, this is only typically possible for few exceptional cases and so it is generally necessary to rely on numerical approaches (e.g., via Monte Carlo simulations) to calculate the precise percolation thresholds via a finite-size scaling analysis on finite lattices. In this regard, from a point of view of numerical simulations, significant algorithmic progress has been made by using bookkeeping concepts based on union-find data structures [16] that led to highly-efficient algorithms for bond and site percolation problems [17, 18]. For an extension of the algorithmic procedure to continuum percolation models, describing spatially-extended, randomly-oriented and possibly overlapping objects, see Ref. [19].

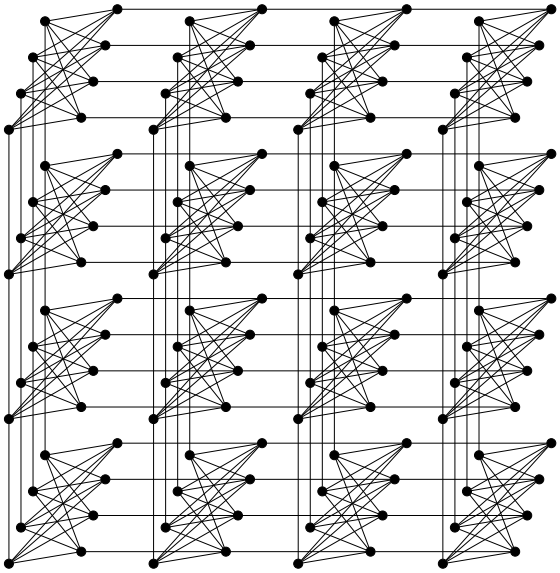

FIG. 1: Topological representation of a Chimera graph with $N = 128$ sites, based on a 4×4 grid of $K_{4,4}$ subgraphs, which corresponds to the D-Wave One Rainier quantum annealer introduced in 2011.

Here, we perform numerical simulations to estimate the thresholds for both bond and site percolation on nonplanar effectively two-dimensional lattices, where the elementary building blocks are given by $K_{n,n}$ subgraphs, i.e., complete bipartite subgraphs of size $2 \times n$ [10] (see Sec. II below for details). The particular choice of $n = 4$ is known as the Chimera graph [20], which is the native (hardware) topology of the special-purpose quantum annealing device developed by D-Wave Systems Inc. [21]. Our motivation to study percolation on the Chimera graph stems from the possible existence of fabrication defects or trapped fluxes that might lead to either malfunctioning qubits (see, for example, Figure 1 in Ref. [22]) or couplers, thus restricting the size of embeddable problems on the D-Wave chip [23]. From an alternative point of view, adopted in the context of network robustness and vulnerability [15, 24], the fraction $f < f_c = 1 - p_c$ might be interpreted as the fraction of sites or bonds that might be absent due to random failures, such as fabrication defects, trapped fluxes or operational errors, while still maintaining large-scale connectivity throughout the chip. Above f_c, however, large-scale connectivity will be lost, leaving small-sized interconnected qubit clusters only. This could also affect the functionality of the chip and become an important issue for particular embeddings of problems where a large fraction of (randomly-chosen) couplers are turned off [25].

There are multiple reasons to compute the percolation threshold of Chimera-like lattices: First, the *native* [26] benchmark problem to study the D-Wave device is an Ising spin glass [27, 28] on the chimera lattice. Because true optima need to be computed using classical simulation techniques to verify that the device can, indeed, find the solutions of the problems, efficient optimization techniques have to be used [29, 30]. Often, not only is the minimum of the cost function needed, but also the ground-state degeneracy. Monte-Carlo-based methods, such as isoenergetic cluster moves [31] have proven to be extremely efficient in studying systems with low ground-state degeneracy, however, to improve the efficiency of the algorithm, it is imperative to know the site percolation threshold of the underlying lattice. Simple subgraphs with known ground states, such as one-dimensional graphs [32, 33] and spanning trees [34], have been investigated on the D-Wave device. In addition, there have been attempts to create hard benchmark problems using planted solutions [35]. While these elegant approaches have the advantage that the solution to the problem to be optimized is known a priori, the used construction procedures might lead to diluted graphs in which only a finite fraction of edges on the lattice are used. Although the construction procedure contains correlations and the adding of edges is not purely random, the problem shares characteristics of random bond percolation and so disconnected clusters might occur. Finally, next-generation hardware might likely include a more interconnected topology, i.e., larger values of n in the $K_{n,n}$ building blocks. Understanding the possible failure rate of these more complex architectures due to percolation is of great importance in the design and scalability of future-generation devices.

Here, we numerically study the $K_{4,4}$-based Chimera lattice with up to $N \approx 20\,000$ sites and estimate the site-percolation threshold by performing a finite-size scaling of the Binder parameter [36] to be $p_c \approx 0.3866(3)$ (see also the Supplementary Material of Ref. [31]). In addition, we study general $K_{n,n}$-based Chimera-like lattices with $n = 2, \ldots, 8$ and estimate the corresponding bond- and site-percolation thresholds $p_{c,n}$, as well as the associated critical exponents that describe the percolation transition.

The paper is organized as follows. In Sec. II we introduce Chimera graphs in more detail, followed by details of the simulations in Sec. III and results in Sec. IV. We summarize and discuss our findings in Sec. V.

II. THE CHIMERA TOPOLOGY

We consider nonplanar, effectively two-dimensional lattice graphs $G = (V, E)$, consisting of a vertex set V, containing $N \equiv v(G)$ vertices, and an edge set E, containing $M \equiv e(G)$ undirected edges. The elementary building blocks of these graphs are $K_{n,n}$ subgraphs, i.e., complete bipartite graphs [10, 37] containing $2 \times n$ sites. These subgraphs can be partitioned into two vertex subsets V_1 and V_2 of size $v_1 = v_2 = n$ and have an edge set, consisting of all possible $v_1 \times v_2$ undirected edges with one terminal vertex in V_1 and one in V_2.

To compose the full Chimera graph G with $N = 2 \times n \times L_x \times L_y$ vertices, $K_{n,n}$ subgraphs are arranged on a $L_x \times L_y$ grid. For horizontally (vertically) adjacent subgraphs $K_{n,n}$ and $K'_{n,n}$, and following an ordering of the vertices in the respective vertex subsets $V_{1,2}$ and $V'_{1,2}$, vertices out of V_1 (V_2) are joined to their respective mirror-vertex in V'_1 (V'_2). The particular choice with $n = 4$ yields the canonical Chimera graph. A topological representation of such a Chimera graph with $L_x = L_y = 4$ is shown in Fig. 1.

Subsequently, we consider Chimera-like graphs of size $N = 8192$ ($L_x = L_y = 32$) up to $N = 294912$ ($L_x = L_y = 192$) in order to perform a finite-size scaling analysis for different subgraph sizes and to determine the respective thresholds for bond, as well as site percolation. Note that there is a difference between the practical (small) graph sizes to which the D-Wave chip architecture is currently limited to (see Ref. [21]), as opposed to large systems that, from a point of view of statistical physics, display a decent finite-size scaling behavior. Given that between 2011 and 2015 the number of sites increased from $N = 128$ (Rainier chip, see Fig. 1) to $N = 1152$ (Washington chip) on the D-Wave device, we can expect [38] to see chips of the order of sites studied in this work by 2019.

III. NUMERICAL DETAILS

For the numerical simulations we use the highly-efficient algorithm by Newman and Ziff [17, 18] based on a union-find data structure [16]. In particular, we implemented union-by-rank and path-compression for the find-part of the bookkeeping procedure.

Within the bond-percolation study, one sweep of the algorithm goes as follows: First, a random permutation of the

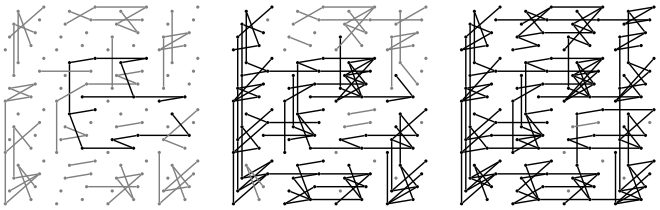

FIG. 2: Instances of bond percolation configurations on a Chimera graph with $N = 128$ sites. From left to right: $p = 0.2$, $p = 0.38 \approx p_c$, and, $p = 0.42$. The vertices and edges belonging to the largest connected component are colored black and the remaining vertices and subsisting edges are colored gray.

TABLE I: Critical parameters of bond percolation (BP) and site percolation (SP) for $n = 4$ Chimera graphs. From left to right: Critical percolation threshold p_c, critical exponents ν and β (obtained from a finite-size scaling of the order parameter), as well as γ (obtained from the order parameter fluctuations and the scaling behavior of the average size of the finite clusters). For details see the main text.

Type	p_c	ν	β	γ
BP	0.2943(1)	1.34(2)	0.146(8)	2.42(2)
SP	0.38722(7)	1.34(3)	0.145(5)	2.41(2)

edges in the edge set E of G is obtained by means of a Fisher-Yates shuffle [16] [having algorithmic complexity $\mathcal{O}(M)$ with M the number of edges]. Initially, each vertex is its own single-site cluster. Edges from the shuffled edge set are added one at a time and for each edge it is checked whether its incident vertices belong to different clusters. If this is the case, the respective clusters are merged using the union-by-rank approach. Once all edges have been probed, one lattice sweep is completed. We measure the size of the largest cluster and the average size of all finite clusters. Because of the previously-described approach, these can be measured very efficiently with a resolution of $\Delta p = 1/M$. However, to keep the amount of raw-data manageable, we consider only approximately 80 values of p in the vicinity of the critical point. Error bars are computed by averaging over 5×10^4 sweeps for each system size studied.

Note that while the bond percolation variant of the algorithm only requires an edge list representing E—i.e., the edge set of the underlying graph—the site percolation variant of the algorithm relies on an adjacency list of G, i.e., a collection of lists of neighbors for each node [16].

IV. RESULTS

We illustrate our approach and data analysis in detail using a finite-size scaling analysis of the canonical $K_{4,4}$-based Chimera lattice. However, we have performed the same algorithm for all $K_{n,n}$ lattices with $n = 2, \ldots, 8$.

A. Bond percolation on $n = 4$ Chimera graphs

The observables we consider can be rescaled following a generic scaling assumption, i.e.,

$$y(p, N) = N^{-b/2}\, f[(p - p_c)N^{1/(2\nu)}], \tag{1}$$

where ν and b represent dimensionless critical exponents (or ratios thereof, see below), p_c is the critical threshold, and $f[\cdot]$ denotes an unknown scaling function [9, 39]. Following Eq. (1), data curves of the observable $y(p, N)$ computed at different values of p and N fall on top of each other, if the scaling parameters p_c, ν, and b are chosen properly. The values of the scaling parameters that yield the best data collapse determine the numerical values of the critical point and the critical exponents that govern the behavior of the underlying observable $y(p, N)$.

To determine the optimal data collapse for a given set of data curves we perform a computer-assisted scaling analysis [40, 41]. Here, the "quality" of the data collapse is measured by the mean-square distance of the data points to the master scaling curve S, described by the scaling function, in units of the standard error of the data points [42]. It is a quantitative measure for the quality of a data collapse that is far superior than the commonly used eyeballing scaling analysis. It is common practice to limit the analysis to the larger system sizes, for which corrections to scaling are less pronounced, and to discard small system sizes that are typically affected by stronger systematic corrections to scaling [39]. In general, systematic corrections to scaling result in a scaling behavior that deviates from that predicted by the scaling assumption, Eq. (1). Note that such corrections are not taken into account here. Furthermore, while S can be influenced by potential corrections to scaling, it might not be interpreted as a measure for these corrections. Here, if not stated explicitly, the scaling analysis is limited to the three largest systems simulated.

Example instances of bond percolation configurations in the subcritical, critical and supercritical regime for Chimera graphs with $N = 128$ sites are shown in Fig. 2. The resulting numerical estimates of the critical percolation thresholds and corresponding critical exponents for bond and site percolation are listed in Tab. I.

1. *Analysis of the Binder ratio*

First we consider the relative size of the largest cluster of connected vertices $s_{\max}$. The dimensionless ratio, known as the Binder parameter [43], is defined via

$$b(p) = \frac{1}{2}\left[3 - \frac{\langle s^4_{\max}(p)\rangle}{\langle s^2_{\max}(p)\rangle^2}\right]. \tag{2}$$

Here, $\langle \cdots \rangle$ represents an average over sweeps. Because the system-size dependent part of the scaling function in Eq. (1) cancels out in the Binder ratio, it has a simple scaling form that follows Eq. (1) with $b = 0$. When $p = p_c$ the argument of the scaling function f is zero and thus system-size independent. This means that data for different system sizes N

cross at $p = p_c$; see inset to Fig. 3(a). Determining the correct thermodynamic values of p_c and ν results in a data collapse, as can be seen in the main panel of Fig. 3(a). There are visible corrections to scaling in the nonpercolating phase, i.e., for $p < p_c$. To account for this, the scaling analysis is performed in the interval $\epsilon \in [-0.25, 1.75]$ on the rescaled p-axis to accentuate the region where $b(p)$ scales well. Consequently, the best data collapse yields $p_c = 0.2946(2)$ and $\nu = 1.34(2)$ with a quality $S = 1.10$ of the data collapse [44]. Note that the numerical value of the correlation length exponent ν is in good agreement with $\nu = 4/3 \approx 1.333$, the standard value for percolation in two-dimensional lattices.

2. *Analysis of the order parameter*

The scaling of the disorder-averaged order parameter

$$P_{\max}(p) = \langle s_{\max}(p) \rangle, \tag{3}$$

is expected to follow Eq. (1) with $b = \beta/\nu$. Here, β refers to the percolation strength exponent that governs the growth of the largest cluster with increasing system size at fixed $p = p_c$. The best data collapse (obtained in the range $\epsilon \in [-0.5, 0.5]$) yields $p_c = 0.2943(1)$, $\nu = 1.37(4)$, and $\beta = 0.146(8)$ with a quality $S = 1.10$, see Fig. 3(b). If we fix the numerical values of the critical exponents to their exact values for two-dimensional percolation ($\nu = 4/3 \approx 1.333$ and $\beta = 5/36 \approx 0.139$) we are left with only one adjustable parameter, resulting in the estimate $p_c = 0.2944(6)$ with (expectedly worse) collapse-quality $S = 4.5$. However, both numerical values are still in good agreement.

3. *Analysis of the order parameter fluctuations*

A third critical exponent can be estimated from the scaling of the order parameter fluctuations $\chi(p)$, i.e.,

$$\chi(p) = N[\langle s^2_{\max}(p) \rangle - \langle s_{\max}(p) \rangle^2]. \tag{4}$$

The fluctuations $\chi(p)$ are expected to scale according to Eq. (1) allowing one to determine the fluctuation exponent γ through $b = -\gamma/\nu$. Here, so as to perform the best possible data-collapse, the nonsymmetric range $\epsilon \in [-0.3, 1.0]$ is chosen. This is motivated by the observation that the peaks of the data curves are located in the super-percolating regime, with the precise location of the peaks approaching their asymptotic value from above. Hence the aforementioned asymmetric interval accentuates the region around the peaks, resulting in the estimates $p_c = 0.2944(2)$, $\nu = 1.33(1)$, and $\gamma = 2.42(2)$ with a quality $S = 0.74$, see Fig. 3(c) for a scaling collapse. Note that the numerical value of the fluctuation exponent is in reasonable agreement with the expected exact value for two-dimensional percolation, namely $\gamma = 43/18 \approx 2.389$.

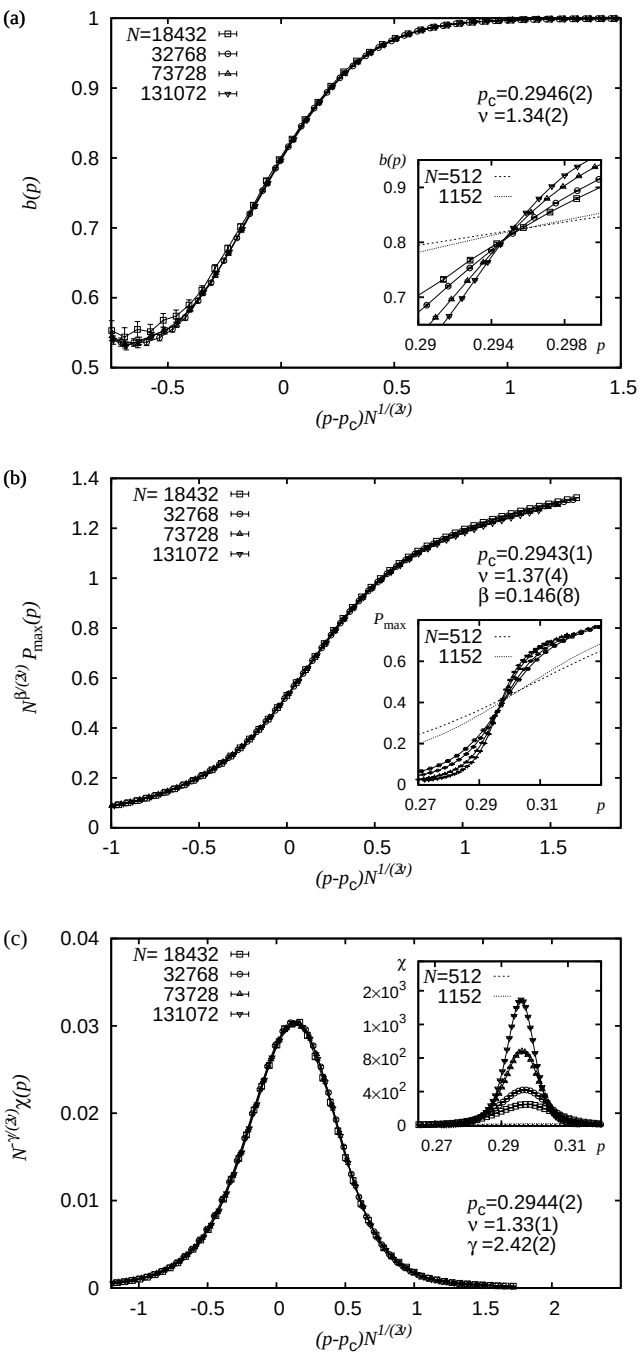

FIG. 3: Finite-size scaling analysis of the relative size $s_{\max}$ of the largest cluster of sites for the bond-percolation problem on Chimera graphs. The main panels always show the scaled data according to Eq. (1), whereas the insets display the unscaled data in the vicinity of the critical point. (a) Binder ratio $b(p)$, (b) disorder-averaged order parameter $P_{\max}(p)$, and, (c) fluctuation $\chi(p) = N \times \mathrm{var}(s_{\max})$ of the order parameter. Note that the insets feature two additional data curves, illustrating the statistical properties of small Chimera graphs of current quantum annealing machines with $N = 512$ $N = 1152$ qubits/sites.

B. Site percolation on Chimera graphs

The analysis of the site-percolation problem is analogous to the analysis performed for bond percolation (Sec. IV A). Note that, as discussed in Ref. [31], the location of the site-percolation threshold is pivotal for the efficient and correct performance of cluster algorithms designed to simulate spin-glass models in arbitrary space dimensions. In Ref. [31], the authors simulated Chimera lattices with up to $N = 20\,000$ sites, and estimated the site-percolation threshold from the finite-size scaling of the Binder parameter, finding $p_c \approx 0.3866(3)$ with $\nu = 1.39(1)$.

We perform an analysis of the order parameter using systems of up to $N = 294912 = 8 \times 192^2$ sites. By increasing the system sizes by approximately one order of magnitude in comparison to the study of Ref. [31] we are able to verify that the exponent ν is very likely in the two-dimensional percolation universality class. From an analysis of the Binder ratio we obtain $p_c = 0.3871(1)$, which, compared to the estimate of Ref. [31], turns out to be slightly larger.

Although the associated critical exponent $\nu = 1.33(2)$ is in good agreement with the two-dimensional percolation value, the data-collapse quality $S = 3.73$ is rather large, reflecting that there are deviations from the expected scaling behavior, similar to the difficulties encountered in the analysis of bond percolation in Sec. IV A.

To ensure that our analysis of the order parameter and its fluctuations is as precise as possible, we increased the number of samples studied to 5×10^5. Our estimates of the critical parameter for site percolation on the $K_{4,4}$-based Chimera lattice are $p_c = 0.38722(7)$, $\nu = 1.34(3)$, $\beta = 0.145(5)$ ($\epsilon = [-0.20 : 0.20]$; $S = 1.00$). Furthermore, the parameter estimates obtained from the order parameter fluctuations are $p_c = 0.3870(2)$, $\nu = 1.34(1)$, $\gamma = 2.41(2)$ ($\epsilon = [-0.70 : 0.70]$; $S = 2.50$). Note that both estimates of p_c are in agreement with each other and in agreement with the Binder cumulant values estimated above. In both cases, the critical exponent ν is in agreement with the exact value of two-dimensional percolation and β and γ are in reasonable agreement with their exact two-dimensional values (i.e., within two standard deviations). Despite the numerical values of β and γ not matching the known values of 2D percolation exactly, we believe, based on the other exponents and our general expectations on this short-ranged percolation model, that the transition is actually of the universality class of 2D random percolation.

C. Percolation thresholds on generalized Chimera graphs

For $K_{n,n}$-based generalized Chimera graphs one might intuitively expect that the percolation threshold is a decreasing function of the average vertex degree and thus of n (however, note that counterexamples can be constructed [45] on planar lattices). Here, we perform a finite-size scaling analysis for the disorder-averaged relative size of the largest cluster, i.e., the order parameter [Eq. (3)], to determine the thresholds for $n = 2$ through 8 (the standard Chimera graph has $n = 4$). Therefore, for each value of n, we consider three system sizes with up to $N = 131044$ sites (the precise value of N depends of the choice of n, of course). Furthermore, we consider 10^4 different permutations of the edge set or the vertex set for both bond and site percolation to compute $\langle s_{\max}(p) \rangle$. As can be seen in Fig. 4, the thresholds decrease with increasing n and can be fit well by functions of the form $f(n) = a \cdot (n - \Delta n)^{-b}$. In this regard we find $a = \mathcal{O}(1)$, $\Delta n = \mathcal{O}(1)$ and $b \approx 1$ [$b \approx 0.5$] for bond [site] percolation. For the bond-percolation variant one might further rephrase this scaling in terms of the number of internal $K_{n,n}$ edges, i.e., $m = n^2$, to also find a scaling with a characteristic exponent $b \approx 0.5$. In either case, this suggests that in the asymptotic limit, $p_c \to 0$ as $n \to \infty$. The results of the finite-size scaling analysis are listed in Tab. II, (the results for the canonical Chimera lattice are again listed for $n = 4$).

The quality of the data collapse is somewhat sensitive to the scaling interval ϵ chosen in the course of the analysis. For example, for the critical point $p_{c,2}$ for site percolation on the $K_{2,2}$ Chimera graph we obtained estimates in the range $p_{c,2} = 0.5124(1)$ ($\epsilon = [-1.00 : 0.75]$; $S = 1.54$) to $p_{c,2} = 0.5129(2)$ ($\epsilon = [-0.50 : 0.50]$; $S = 1.97$). Generally, we expect that a narrower scaling interval ϵ—enclosing the critical point without extending too far into the off-critical region where deviations from the scaling behavior are expected—should lead to a more reliable estimate of p_c. For example, for the given statistics (e.g., 10^4 samples), restricting the scaling interval further to the range $\epsilon = [-0.20 : 0.30]$ results in $p_{c,2} = 0.51301(15)$, $\nu = 1.32(5)$ and $\beta = 0.145(7)$ ($S = 1.84$). The scaling exponents are also in agreement with the exact two-dimensional values. Increasing the statistics by a factor of 10 to 10^5 independent samples effectively allows us to add one digit of precision, i.e., $p_{c,2} = 0.51294(7)$ ($\epsilon = [-0.30 : 0.30]$; $S = 0.30$), a result that is in good agreement with an independent estimate by R. Ziff [46].

What does this mean for architectures built from $K_{n,n}$ subgraphs? From a point of view of network robustness and vulnerability, increasing n leads to a hardware topology that is less vulnerable to a random failures of qubits. For example, while the native D-Wave design with $n = 4$ allows for a random failure of approximately 62% of the qubits (70% of the

TABLE II: Percolation thresholds on generalized Chimera graphs built from $K_{n,n}$ elementary cells of size $n = 2$ through 8. From left to right: Size n of the $K_{n,n}$ elementary cell (each cell contains $2n$ sites), critical points $p_{c,n}$ obtained from an analysis of the order parameter for bond percolation (BP) and site percolation (SP), respectively.

n	$p_{c,n}$ (BP)	$p_{c,n}$ (SP)
2	0.44778(15)	0.51294(7)
3	0.35502(15)	0.43760(15)
4	0.29427(12)	0.38675(7)
5	0.25159(13)	0.35115(13)
6	0.21942(11)	0.32232(13)
7	0.19475(9)	0.30052(14)
8	0.17496(10)	0.28103(11)

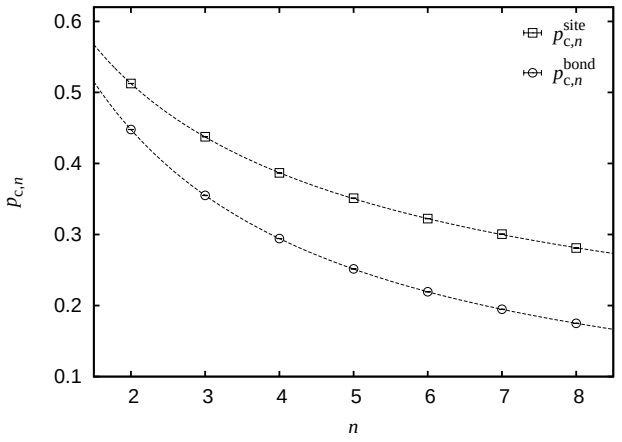

FIG. 4: Bond and site percolation thresholds for Chimera-like graphs built from $K_{n,n}$ subgraphs. The percolation thresholds decrease with increasing average vertex degree and thus of n, the cell size. The dashed lines represent fits to functions of the form $f(n) = a \cdot (n - \Delta n)^{-b}$ (see text for details).

couplers) without losing large-scale connectivity, this value rises to about 72% (83% in case of couplers) if the size of the elementary building blocks is scaled up only by a factor of 2 to $n = 8$. Therefore, using topologies that have high connectivity or, for example, small-world properties [47] is key in designing quantum annealing machines robust to random failures of qubits and couplers.

D. Small-world enhanced Chimera graphs

We now discuss how to improve the stability of Chimera-like lattices by merely increasing the average degree by one via the addition of $N/2$ "small-world" (SW) bonds to the existing regular Chimera graph. This results in a super-graph G' of G, which we refer to as a small-world Chimera graph (SWCG). Our aim is to determine the location of the site-percolation threshold for the ensemble of SWCGs and to assess the gain in network robustness. The additional SW bonds that make up an instance of a SWCG are obtained by the following three-step procedure: (i) generate a list of N integers that represent the vertices of the (plain) Chimera graph, (ii) obtain a random permutation of the list, and, (iii) interpret subsequent pairs of integers as the end-vertices of $N/2$ additional bonds that, in turn, are added to the initial graph. In doing so, the degree of each vertex increases by *exactly* one [48]. The resulting percolation thresholds can be expected to decrease with decreasing average degree, and, consequently, the ensemble of SWCGs can be expected to be less vulnerable to random qubit failures. This is in agreement with the containment principle due to Fisher [4], stating that if G results from G' by removing a fraction of its bonds (i.e., G being a spanning subgraph of G', see Ref. [10]), then $p_c^{G'} \leq p_c^G$ for *both* bond and site percolation.

For the SWCGs, it is anticipated that there is a scaling window around p_c that has mean-field exponents. A proof of such scaling window exists on quasi-random graphs [49]. Figure 5 illustrates a finite-size scaling analysis of the order parameter and its associated finite-size susceptibility for the site-percolation problem on SWCGs. In the vicinity of the critical point we expect the unscaled order parameter data to scale as

$$P_{\max}(p) \sim |p - p_c|^{\beta}. \tag{5}$$

From the data corresponding to different system sizes, we obtain the system-size-dependent effective estimates $p_c(N)$ and $\beta(N)$. From the effective critical points we extrapolate to the asymptotic critical point p_c^∞ by fitting the data to

$$p_c = p_c^\infty + aN^{-b}, \tag{6}$$

with $p_c^\infty = 0.207(4)$, $a = 0.5(3)$, and $b = 0.32(9)$, as shown

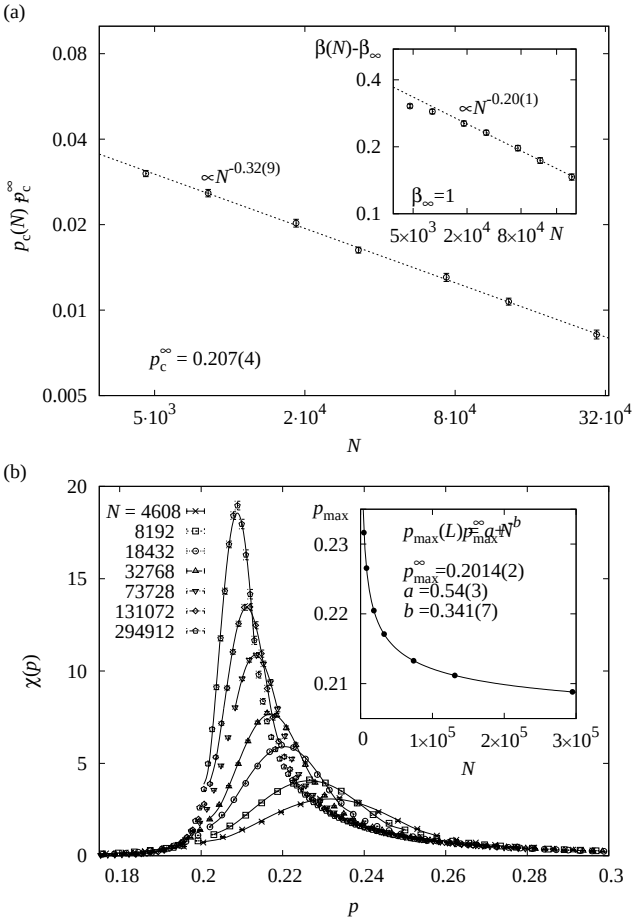

FIG. 5: Finite-size scaling analysis of the relative size $s_{\max}$ of the largest cluster of sites for the site-percolation problem on the small-world enhanced Chimera graphs (see Sec. IV D). Panel (a): Scaling of the effective system-size-dependent estimate of $p_c(N)$. The inset shows a scaling of $\beta(N)$, as discussed in the text. Panel (b): Fit of 5th-order polynomials to the finite-size fluctuations to estimate the system-size-dependent peak positions $p_{\max}(N)$. The inset shows the extrapolation to the asymptotic critical point $p_{\max}^\infty$, as discussed in the text.

in the main plot of Fig. 5(a). Similarly, the sequence of exponents $\beta(N)$ is fit well by

$$\beta(N) = \beta_\infty + aN^{-b}, \tag{7}$$

where $\beta_\infty = 1.20(16)$, $a = -1.21(7)$, and $b = 0.10(4)$ if the fit is restricted to systems of size $N > 10^4$. Upon successively excluding the smaller system sizes from the fit we find that the value of β_∞ approaches the expected mean-field value $\beta = 1$ [50]. For example, restricting the analysis to $N > 2 \times 10^4$ yields $\beta_\infty = 1.06(7)$, $a = -1.5(4)$, and $b = 0.16(4)$, see the inset of Fig. 5(a). Note that in the figure we fixed $\beta_\infty = 1$.

An additional estimate of the critical point can be obtained from the position of the peaks of the finite-size susceptibility $\chi(p)$. We have located the individual peak positions $p_{\max}(N)$ by fitting a polynomial of 5th order to the unscaled data curves. This is illustrated in Fig. 5(b), where the main plot shows the raw data with the respective fits and the inset shows the scaling behavior of the peak-positions, where a fit to the function

$$p_{\max}(N) = p_{\max}^\infty + aN^{-b} \tag{8}$$

yields $p_{\max}^\infty = 0.2014(2)$, $a = 0.54(3)$, and $b = 0.341(7)$. The value of $p_{\max}^\infty$ is in reasonable agreement with the above estimate based on the analysis of the order parameter. Furthermore, the numerical value of the critical point compares well with an estimate $p_c = 0.201(1)$ obtained using a data-collapse analysis (not shown).

Note that both estimates, p_c^∞ and $p_{\max}^\infty$ are in reasonable agreement and are located significantly below the threshold value $p_c = 0.38675(7)$ of the standard Chimera graph. Consequently, SWCGs provide a topology that is significantly less vulnerable to random failures of qubits, i.e., while the standard Chimera graph exhibits a fragmentation threshold $f_c = 1 - p_c \approx 0.62$ and thus allows for a random failure of approximately 62% of the qubits without losing large scale connectivity, this value increases to $f_c \approx 0.80$ for the ensemble of SWCGs. Finally, we note that the critical exponents for percolation on SWCGs assume mean-field values when $\mathcal{O}(N)$ small-world bonds are added, as demonstrated in the presented study.

Finally, note that Chimera topologies are the archetypal architecture used in current quantum annealers. While, from a point of view of robustness, a fully-connected topology would be desirable, a hardware implementation seems not possible at present. To be precise, only a finite number of fabrication layers for the chips are available. Having a fully-connected graph would require $O(N)$ layers, which is prohibitive for current chip designs with ~ 1000 qubits. Given the flux qubit structure used in current quantum annealing machines, $K_{n,n}$-like topologies might be used for multiple upcoming generations of these devices.

V. SUMMARY

We have performed numerical simulations to determine the bond- and site-percolation thresholds on nonplanar, effectively two-dimensional lattice graphs, where the elementary building blocks are complete bipartite subgraphs $K_{n,n}$ ($n = 2, \ldots, 8$). The simulations have been performed using a highly efficient percolation algorithm [17, 18] based on a union-find data structure [16]. From a finite-size scaling analysis we have obtained the critical points p_c and the three critical exponents ν, β and γ, thus locating the critical bond- and site-percolation thresholds and allowing us to verify that the transition is in the two-dimensional percolation universality class. In either case, the percolation threshold is a decreasing function of n and our results suggests that in the asymptotic limit $p_c \to 0$ as $n \to \infty$.

The particular choice of $n = 4$ is the canonical Chimera graph, i.e., the hardware topology of the D-Wave quantum annealing device, developed at D-Wave Systems Inc. [21]. The native (no embedding required) benchmark (optimization) problem for the D-Wave device is an Ising spin glass [27, 51] and recently, much effort was put into the simulation of Ising spin glasses on the Chimera topology [29, 30, 52]. As discussed in Ref. [31], the location of the site-percolation threshold is crucial for the efficient and correct performance of cluster algorithms designed to simulate spin-glass models on, e.g., the above graph topology.

Finally, referring to the implementation of, e.g., the D-Wave chip and adopting the point of view of network robustness and vulnerability, the above results suggest that the native D-Wave design, as analyzed in Secs. IV A and IV B, allows for a random failure of approximately 62% of the qubits (70% of the couplers) prior to losing large-scale connectivity on the chip. Similarly, embedded problems that turn off a sizable fraction of couplers randomly, might lead to loss of connectivity. Bear in mind that the above figures are valid in the asymptotic limit. In general, for finite-sized graphs of no more than 10^3 sites, finite-size effects result in effective thresholds that differ slightly from the asymptotic values quoted in Table II. To illustrate this, one might, e.g., define effective, system-size dependent critical points from the peak locations of the finite-size fluctuations χ (see Sec. IV A 3). In this regard, for bond [site] percolation on a lattice with $N = 512$ sites we observe $p_{\chi-\max}(N = 512) \approx 0.307$ [$p_{\chi-\max}(N = 512) \approx 0.408$], i.e., shifting towards smaller values as $N \to \infty$. Similarly, for $N = 1152$, $p_{\chi-\max}(N = 1152) \approx 0.304$ for bond percolation and $p_{\chi-\max}(N = 1152) \approx 0.403$ for site percolation. Finally, for the largest system sizes studied in this work, $p_{\chi-\max}(N = 131072) \approx 0.296$ for bond percolation and $p_{\chi-\max}(N = 294912) \approx 0.389$ for site percolation. Although the asymptotic peaks seem to be located slightly above p_c (within the superpercolating regime), this might nevertheless lead to expect that the finite-size values of p_c for bond and site percolation for the $N = 1152$ Chimera graph are within a 5% interval of the asymptotic critical point.

In addition, we have found that by extending the plain $K_{4,4}$-based Chimera graph using $N/2$ small-world bonds—thereby effectively increasing the average vertex-degree by one—the respective percolation threshold decreases to $p_c = 0.207(4)$. Thus, small-world-extended Chimera graphs provide a topology that allows for a random failure of approximately 80% of the qubits before the large-scale connectivity of the device is

lost. As pointed out earlier, using topologies that have higher connectivity, such as the above extended Chimera graphs, might be key in designing quantum annealing machines robust to random failures of qubits and couplers.

Acknowledgments

We would like to thank R. Ziff for sharing his estimates of $p_{c,2}$ with us, as well as fruitful discussions. O. M. thanks Zheng Zhu for valuable discussions and comments, as well as for critically reading the manuscript. Furthermore, he thanks Juan Gabriel Ochoa for attentively listening to mostly one-sided monologues while waiting for the numerical simulations to complete. H. G. K. thanks Firas Hamze for comments and discussions and acknowledges support from the National Science Foundation (Grant No. DMR-1151387). He would also like to thank Jacques and Spock Tran for providing an enjoyable working environment. H. G. K.'s and O.M.'s research is based in part upon work supported in part by the Office of the Director of National Intelligence (ODNI), Intelligence Advanced Research Projects Activity (IARPA), via MIT Lincoln Laboratory Air Force Contract No. FA8721-05-C-0002. The views and conclusions contained herein are those of the authors and should not be interpreted as necessarily representing the official policies or endorsements, either expressed or implied, of ODNI, IARPA, or the U.S. Government. The U.S. Government is authorized to reproduce and distribute reprints for Governmental purpose notwithstanding any copyright annotation thereon. M. A. N. is supported in part by a grant from Pacific Northwest National Laboratory (PNNL).

[1] S. R. Broadbent and J. M. Hammersley, *Percolation processes. I. Crystals and Mazes*, Proceedings of the Cambridge Philosophical Society **53**, 629 (1957).

[2] Hammersley, J. M., *Percolation Processes: Lower Bounds for the Critical Probability*, Ann. Math. Statist. **28**, 790 (1957).

[3] J. M. Hammersley, *Percolation processes. II. The connective constant*, Proceedings of the Cambridge Philosophical Society **53**, 642 (1957).

[4] M. E. Fisher, *Critical Probabilities for Cluster Size and Percolation Problems*, J. Math. Phys. **2**, 620 (1961).

[5] A. Bunde, P. Maass, and M. D. Ingram, *Diffusion Limited Percolation: A Model for Transport in Ionic Glasses*, Berichte der Bunsengesellschaft für physikalische Chemie **95**, 977 (1991).

[6] F. O. Pfeiffer and H. Rieger, *Superconductor-to-normal phase transition in a vortex glass model: numerical evidence for a new percolation universality class*, J. Phys. Cond. Mat. **14**, 2361 (2002).

[7] F. O. Pfeiffer and H. Rieger, *Critical properties of loop percolation models with optimization constraints*, Phys. Rev. E **67**, 056113 (2003).

[8] D. Stauffer, *Scaling theory of percolation clusters*, Phys. Rep. **54**, 1 (1979).

[9] D. Stauffer and A. Aharony, *Introduction to Percolation Theory* (Taylor and Francis, London, 1994).

[10] J. W. Essam and M. E. Fisher, *Some Basic Definitions in Graph Theory*, Rev. Mod. Phys. **42**, 271 (1970).

[11] J. M. Yeomans, *Statistical Mechanics of Phase Transitions* (Oxford University Press, Oxford, 1992).

[12] A. M. Becker and R. M. Ziff, *Percolation thresholds on two-dimensional Voronoi networks and Delaunay triangulations*, Phys. Rev. E **80**, 041101 (2009).

[13] A. A. Saberi, *Recent advances in percolation theory and its applications*, Physics Reports **578**, 1 (2015).

[14] M. E. J. Newman, S. H. Strogatz, and D. J. Watts, *Random graphs with arbitrary degree distributions and their applications*, Phys. Rev. E **64**, 026118 (2001).

[15] D. S. Callaway, M. E. J. Newman, S. H. Strogatz, and D. J. Watts, *Network Robustness and Fragility: Percolation on Random Graphs*, Phys. Rev. Lett. **85**, 5468 (2000).

[16] T. H. Cormen, C. E. Leiserson, R. L. Rivest, and C. Stein, *Introduction to Algorithms, 2nd edition* (MIT Press, Cambridge, MA, 2001).

[17] M. E. J. Newman and R. Ziff, *Efficient Monte Carlo Algorithm and High-Precision Results for Percolation*, Phys. Rev. Lett. **85**, 4104 (2000).

[18] M. E. J. Newman and R. Ziff, *Fast Monte Carlo algorithm for site or bond percolation*, Phys. Rev. E **64**, 016706 (2001).

[19] S. Mertens and C. Moore, *Continuum percolation thresholds in two dimensions*, Phys. Rev. E **86**, 061109 (2012).

[20] P. Bunyk, E. Hoskinson, M. W. Johnson, E. Tolkacheva, F. Altomare, A. J. Berkley, R. Harris, J. P. Hilton, T. Lanting, and J. Whittaker, *Architectural Considerations in the Design of a Superconducting Quantum Annealing Processor*, IEEE Trans. Appl. Supercond. **24**, 1 (2014).

[21] URL `http://www.dwavesys.com`.

[22] Z. Bian, F. Chudak, R. Israel, B. Lackey, W. G. Macready, and A. Roy, *Discrete optimization using Quantum Annealing on sparse Ising models*, Frontiers in Physics **2** (2014).

[23] C. Klymko, B. D. Sullivan, and T. S. Humble, *Adiabatic quantum programming: minor embedding with hard faults*, Quant. Inf. Proc. **13**, 709 (2014).

[24] R. Albert, H. Jeong, and A. Barabási, *Error and attack tolerance of complex networks*, Nature **406**, 378 (2000).

[25] Note that in Ref. [53] the percolation properties of a 2-level-grid minor-embedded into Chimera were studied within the context of quantum annealing corrections.

[26] Within this context, *native* refers to a problem that uses all physical qubits on the chip as logical qubits. An embedded problem, for example, might require multiple physical qubits to encode one logical qubit or interaction between two qubits that are not nearest neighbors on the lattice.

[27] K. Binder and A. P. Young, *Spin Glasses: Experimental Facts, Theoretical Concepts and Open Questions*, Rev. Mod. Phys. **58**, 801 (1986).

[28] D. L. Stein and C. M. Newman, *Spin Glasses and Complexity*, Primers in Complex Systems (Princeton University Press, 2013).

[29] H. G. Katzgraber, F. Hamze, and R. S. Andrist, *Glassy Chimeras Could Be Blind to Quantum Speedup: Designing Better Benchmarks for Quantum Annealing Machines*, Phys. Rev. X **4**, 021008 (2014).

[30] H. G. Katzgraber, F. Hamze, Z. Zhu, A. J. Ochoa, and H. Munoz-Bauza, *Seeking Quantum Speedup Through Spin Glasses: The Good, the Bad, and the Ugly*, Phys. Rev. X **5**,

031026 (2015).
[31] Z. Zhu, A. J. Ochoa, and H. G. Katzgraber, *Efficient Cluster Algorithm for Spin Glasses in Any Space Dimension*, Phys. Rev. Lett. **115**, 077201 (2015).
[32] I. Hen, J. Job, T. Albash, T. F. Rønnow, M. Troyer, and D. A. Lidar, *Probing for quantum speedup in spin-glass problems with planted solutions*, Phys. Rev. A **92**, 042325 (2015).
[33] A. D. King, *Performance of a quantum annealer on range-limited constraint satisfaction problems* (2015), arXiv:1502.02098.
[34] *A Study of Spanning Trees on a D-Wave Quantum Computer*, Physics Procedia **68**, 56 (2015).
[35] S. Boixo, T. F. Rønnow, S. V. Isakov, Z. Wang, D. Wecker, D. A. Lidar, J. M. Martinis, and M. Troyer, *Evidence for quantum annealing with more than one hundred qubits*, Nat. Phys, **10**, 218 (2014).
[36] K. Binder, *Critical properties from Monte Carlo coarse graining and renormalization*, Phys. Rev. Lett. **47**, 693 (1981).
[37] Note that in Ref. [10] these bipartite graphs are referred to as "bichromatic.".
[38] Needless to mention, the expectation that the current chip topology will scale to hundreds of thousands of qubits requires an unhealthily-large amount of wishful thinking. This estimate does not take into account, for example, fabrication limitations, nor the effects of qubit noise that are amplified the more qubits are added to the system [54–56].
[39] K. Binder and D. W. Heermann, *Monte Carlo simulation in statistical physics: an introduction (4th ed.)* (Springer (Springer series in solid-state science), 2002).
[40] O. Melchert, *autoScale.py - A program for automatic finite-size scaling analyses: A user's guide*, Preprint: arXiv:0910.5403v1 (2009), the source-code of autoScale.py and the raw-data for an illustrative example can be downloaded toghether with the source-files of the preprint at http://arxiv.org/abs/0910.5403 by choosing the download-option `Other formats`.
[41] A. Sorge, *pyfssa: v0.2.0* (2015), `pyfssa` is a scientific Python package for algorithmic finite-size scaling analysis at phase transitions.
[42] J. Houdayer and A. K. Hartmann, *Low temperature behavior of two-dimensional Gaussian Ising spin glasses*, Phys. Rev. B **70**, 014418 (2004).
[43] K. Binder, *Finite size scaling analysis of Ising model block distribution functions*, Z. Phys. B **43**, 119 (1981).
[44] The numerical value of S measures the mean-square distance of the data points to the master scaling curve described by the scaling function, in units of the standard error [42].
[45] J. C. Wierman, *Percolation threshold is not a decreasing function of the average coordination number*, Phys. Rev. E **66**, 046125 (2002).
[46] R. Ziff (private communication) drew our attention to his independent estimates of $p_{\mathrm{c},2} \approx 0.42776$ (bond percolation) and $p_{\mathrm{c},2} \approx 0.51298$ (site percolation) on the $K_{2,2}$ Chimera lattice, consistent with the values quoted in Table II.
[47] H. Guclu, G. Korniss, M. A. Novotny, Z. Toroczkai, and Z. Rácz, *Synchronization landscapes in small-world-connected computer networks*, Phys. Rev. E **73**, 066115 (2006).
[48] If N is odd, one qubit does not have a small-world bond.
[49] A. Nachmias, *Mean-field conditions for percolation on finite graphs*, Geometric and Functional Analysis **19**, 1171 (2009).
[50] C. Moore and M. E. J. Newman, *Exact solution of site and bond percolation on small-world networks*, Phys. Rev. E **62**, 7059 (2000).
[51] A. K. Hartmann and H. Rieger, *Optimization Algorithms in Physics* (Wiley-VCH, Berlin, 2001).
[52] M. Weigel, H. G. Katzgraber, J. Machta, F. Hamze, R. S. Andrist, and Octomore Collaboration, *Erratum: Glassy Chimeras could be blind to quantum speedup: Designing better benchmarks for quantum annealing machines [Phys. Rev. X 4, 021008 (2014)]*, Phys. Rev. X **5**, 019901 (2015).
[53] W. Vinci, T. Albash, G. Paz-Silva, I. Hen, and D. A. Lidar, *Quantum annealing correction with minor embedding*, Phys. Rev. A **92**, 042310 (2015).
[54] Z. Zhu, A. J. Ochoa, F. Hamze, S. Schnabel, and H. G. Katzgraber, *Best-case performance of quantum annealers on native spin-glass benchmarks: How chaos can affect success probabilities* (2015), (arXiv:1505.02278).
[55] A. Perdomo-Ortiz, B. O'Gorman, J. Fluegemann, R. Biswas, and V. N. Smelyanskiy, *Determination and correction of persistent biases in quantum annealers* (2015), (arXiv:quant-phys/1503.05679).
[56] A. Perdomo-Ortiz, J. Fluegemann, R. Biswas, and V. N. Smelyanskiy, *A Performance Estimator for Quantum Annealers: Gauge selection and Parameter Setting* (2015), (arXiv:quant-phys/1503.01083).